

$\Lambda_c N$ interaction from lattice QCD and its application to Λ_c hypernuclei

Takaya Miyamoto^{a,b}, Sinya Aoki^{a,b,c}, Takumi Doi^{b,d}, Shinya Gongyo^b,
Tetsuo Hatsuda^{b,d}, Yoichi Ikeda^{b,e}, Takashi Inoue^{b,f}, Takumi Iritani^b,
Noriyoshi Ishii^{b,e}, Daisuke Kawai^g, Keiko Murano^{b,e}, Hidekatsu Nemura^{b,e},
Kenji Sasaki^{a,b}

^a*Center for Gravitational Physics, Yukawa Institute for Theoretical Physics, Kyoto University, Kyoto 606-8502, Japan*

^b*Theoretical Research Division, Nishina Center, RIKEN, Wako 351-0198, Japan*

^c*Center for Computational Sciences, University of Tsukuba, Ibaraki 305-8571, Japan*

^d*iTHEMS Program and iTHES Research Group, RIKEN, Wako 351-0198, Japan*

^e*Research Center for Nuclear Physics (RCNP), Osaka University, Osaka 567-0047, Japan*

^f*Nihon University, College of Bioresource Sciences, Kanagawa 252-0880, Japan*

^g*Department of Physics, Kyoto University, Kyoto 606-8502, Japan*

Abstract

The interaction between Λ_c and a nucleon (N) is investigated by employing the HAL QCD method in the (2+1)-flavor lattice QCD on a $(2.9 \text{ fm})^3$ volume at $m_\pi \simeq 410, 570, 700$ MeV. We study the central potential in 1S_0 channel as well as central and tensor potentials in 3S_1 – 3D_1 channel, and find that the tensor potential for $\Lambda_c N$ is negligibly weak and central potentials in both 1S_0 and 3S_1 – 3D_1 channels are almost identical with each other except at short distances. Phase shifts and scattering lengths calculated with these potentials show that the interaction of $\Lambda_c N$ system is attractive and has a similar strength in 1S_0 and 3S_1 channels at low energies (i.e. the kinetic energy less than about 40 MeV). While the attractions are not strong enough to form two-body bound states, our results lead to a possibility to form Λ_c hypernuclei for sufficiently large atomic numbers (A). To demonstrate this, we derive a single-folding potential for Λ_c hypernuclei from the Λ_c -nucleon potential obtained in lattice QCD, and find that Λ_c hypernuclei can exist for $A \geq 12$ with the binding energies of a few MeV. We also estimate the Coulomb effect for the Λ_c hypernuclei.

Keywords: Charmed baryon interaction, Charmed hypernuclei, Lattice QCD

1. Introduction

The investigation of baryon-baryon interactions is one of the most important subjects to understand properties of hadronic matter. The low-energy nucleon-nucleon (NN) interaction has been severely constrained by the NN scattering data and the properties of finite nuclei [1]. The hyperon-nucleon (YN) and hyperon-hyperon (YY) interactions have also been investigated phenomenologically to reproduce the properties of hypernuclei and hyperon-nucleon scattering data [2]. Such phenomenological interactions are then used to study yet unknown nuclei and also the neutron star interiors.

As a natural extension, it is interesting to investigate charmed hypernuclei, as initiated in Ref. [3] just after the discovery of the Λ_c baryon. Including charm quarks, the one-boson-exchange potential (OBEP) model for the $Y_c N$ ($Y_c = \Lambda_c, \Sigma_c$) was constructed [4], where the couplings are determined by assuming the flavor $SU(4)$, which is an extension of the flavor $SU(3)$ for the YN interaction. The possibility of both Λ_c and Σ_c nuclear bound states was predicted for heavy nuclei [3]. Further studies were carried out in [5, 6, 7]: Based on flavor $SU(4)$ symmetry, the authors made a comparison between the Λ hypernuclei and the Λ_c hypernuclei. Although the depth of the effective potential for Λ_c in the G-matrix calculation is about 2/3 of that for Λ , they found that the number of bound states in Λ_c hypernuclei is larger than that in Λ hypernuclei due to its heavy mass.

However, the charm quark is much heavier than other three quarks (up, down, strange), so that the flavor $SU(4)$ may not give a good description of the $Y_c N$ interaction. Therefore, Ref. [8] has investigated $\Lambda_c N$ interaction with the OBEP model based on the heavy quark effective theory, where the $\Lambda_c N - \Sigma_c N - \Sigma_c^* N$ coupled channel system is considered. It was then found that $\Lambda_c N$ interaction is strong enough to form a 2-body bound state due to effects of these channel couplings, but the results are rather sensitive to the model parameters. Studies within a framework of the constituent quark model [9, 10, 11, 12] have also been attempted to extract the $\Lambda_c N$ interaction. In Ref. [13, 14], the authors have estimated the single particle energy for Λ_c baryon

in several nuclei by using the quark-meson coupling model, and they claim that Λ_c hypernuclei are likely to be formed.

The aim of the present paper is to shed a new light on the problem of the $\Lambda_c N$ interaction from first-principles lattice QCD simulations. For this purpose, the HAL QCD method to analyze the hadron-hadron interactions on the lattice [15, 16, 17] is most suitable. The method has already been applied to various hadron-hadron systems [18, 19, 20, 21, 22, 23] and to hadronic matter [24]. Advantages of this method in the context of the present paper are as follows: (i) Applications to the charmed systems are straightforward, (ii) no phenomenological parameters are involved since it is based on first-principles QCD simulations, and (iii) the resultant $\Lambda_c N$ potential is faithful to the QCD S-matrix below the inelastic threshold, so that we can correctly calculate the $\Lambda_c N$ elastic scattering phase shift.

This paper is organized as follows. In section 2, we present a brief description of the HAL QCD method for the $\Lambda_c N$ system. The numerical setup for this work is summarized in section 3. In section 4, we show our numerical results of the $\Lambda_c N$ potentials in both 1S_0 and 3S_1 – 3D_1 channels. We also discuss properties of the $\Lambda_c N$ interaction through phase shifts and scattering lengths calculated by our potentials. In section 5, we employ the single-folding potential to investigate Λ_c hypernuclei. Summary and conclusions are presented in section 6.

2. HAL QCD method for $\Lambda_c N$ system

In this section, we discuss the HAL QCD method [15] to be applied to the $\Lambda_c N$ system. We start with the equal-time Nambu-Bethe-Salpeter (NBS) wave function in the center-of-mass (CM) frame of two baryons at Euclidean time t ;

$$\psi_{\alpha\beta}^{(W)}(\vec{r})e^{-Wt} = \sum_{\vec{x}} \langle 0 | B_{\alpha}^{(1)}(\vec{r} + \vec{x}, t) B_{\beta}^{(2)}(\vec{x}, t) | B^{(1)}(\vec{k}) B^{(2)}(-\vec{k}), W \rangle, \quad (1)$$

where α, β are the spinor indices, and $B_{\alpha}(\vec{x}, t)$ denotes a local interpolating operator for a baryon B . The state $|B^{(1)}(\vec{k}) B^{(2)}(-\vec{k}), W\rangle$ stands for an energy eigenstate of a two baryon system. Here the total energy is denoted by $W = \sqrt{|\vec{k}|^2 + m_{B^{(1)}}^2} + \sqrt{|\vec{k}|^2 + m_{B^{(2)}}^2}$

with the baryon masses $m_{B(1)}$ and $m_{B(2)}$, and the relative momentum \vec{k} . We employ the local interpolating operators for a nucleon and Λ_c as

$$B_\alpha(x) = \epsilon_{ijk} [q_i^T(x) C \gamma_5 q_j(x)] q_{k,\alpha}(x) \quad (2)$$

where $x = (\vec{x}, t)$, and i, j, k are color indices. C is the charge conjugation matrix defined by $C = \gamma_2 \gamma_4$, and $q = u, d, c$ stands for quark operators for up-, down- and charm-quarks, respectively. Flavor structures of a nucleon and Λ_c are given by

$$N \equiv \begin{pmatrix} p \\ n \end{pmatrix} = \begin{pmatrix} [ud] u \\ [ud] d \end{pmatrix}, \quad (3)$$

$$\Lambda_c = \frac{1}{\sqrt{6}} ([cd] u + [uc] d - 2 [du] c). \quad (4)$$

In the asymptotic region ($r = |\vec{r}| \rightarrow \infty$), the NBS wave function satisfies the Helmholtz equation $[\vec{k}^2 + \vec{\nabla}^2] \psi_{\alpha\beta}^{(W)}(r) \simeq 0$ and its asymptotic behavior for a given orbital angular momentum L and total spin S is denoted as

$$\psi_{LS}^{(W)}(r) \propto e^{i\delta_{LS}(k)} \frac{\sin(kr - L\pi/2 + \delta_{LS}(k))}{kr}, \quad (5)$$

where the “scattering phase shift” $\delta_{LS}(k)$ is determined from the unitarity of the S-matrix in QCD [16, 17]. From the NBS wave function, the potential which reproduces the scattering phase shift is defined through the Schrödinger equation as

$$(E - H_0) \psi_{\alpha\beta}^{(W)}(\vec{r}) = \int d^3r' U_{\alpha\beta;\alpha'\beta'}(\vec{r}, \vec{r}') \psi_{\alpha'\beta'}^{(W)}(\vec{r}'), \quad (6)$$

where $H_0 = -\vec{\nabla}^2/2\mu$ with the reduced mass $\mu = m_{B(1)}m_{B(2)}/(m_{B(1)} + m_{B(2)})$, and $E = k^2/2\mu$ is a kinetic energy of the two baryon system in the CM frame. In this definition, the non-local potential $U(\vec{r}, \vec{r}')$ is energy-independent below the inelastic threshold [16, 17]. In order to handle the non-locality of the potential, we introduce the derivative expansion as [25]

$$U(\vec{r}, \vec{r}') = V(\vec{r}, \vec{\nabla}) \delta^{(3)}(\vec{r} - \vec{r}'), \quad (7)$$

where $V(\vec{r}, \vec{\nabla})$ is then expanded in terms of $\vec{\nabla}$. For example, the leading order of the derivative expansion is given by

$$\begin{aligned} V_{LO}(\vec{r}) &= V_0(\vec{r}) + V_\sigma(\vec{r})(\vec{\sigma}_1 \cdot \vec{\sigma}_2) + V_T(\vec{r})S_{12}, \\ S_{12} &= 3 \frac{(\vec{r} \cdot \vec{\sigma}_1)(\vec{r} \cdot \vec{\sigma}_2)}{|\vec{r}|^2} - (\vec{\sigma}_1 \cdot \vec{\sigma}_2), \end{aligned} \quad (8)$$

where $\vec{\sigma}_i$ is the Pauli matrix acting on the spin index of the i -th baryon. The local potentials V_0 , V_σ and V_T , which give the spin-independent force, the spin-spin force and the tensor force, are commonly used in nuclear physics. The convergence of the derivative expansion can be checked e.g. by changing the energy. For example, the leading order approximation is found to be accurate for $E < 45$ MeV in the case of the NN scattering in quenched QCD with $m_\pi \simeq 530$ MeV [26].

In lattice QCD, the NBS wave functions can be extracted from the baryon four-point correlation function given by

$$G_{\alpha\beta}(\vec{r}, t - t_0) = \sum_{\vec{x}} \langle 0 | B_\alpha^{(1)}(\vec{r} + \vec{x}, t) B_\beta^{(2)}(\vec{x}, t) \overline{\mathcal{J}^{(JP)}}(t_0) | 0 \rangle, \quad (9)$$

where $\overline{\mathcal{J}^{(JP)}}(t_0)$ is the source operator which creates two baryon states with the total angular momentum J and the parity P . Inserting a complete set between the two-baryon operator and the source operator in the Eq. (9), we obtain

$$\begin{aligned} G_{\alpha\beta}(\vec{r}, t - t_0) &= \sum_n \sum_{\vec{x}} \langle 0 | B_\alpha^{(1)}(\vec{r} + \vec{x}, t) B_\beta^{(2)}(\vec{x}, t) | W_n \rangle \langle W_n | \overline{\mathcal{J}^{(JP)}}(t_0) | 0 \rangle + \dots \\ &= \sum_n \psi_{\alpha\beta}^{(W_n)}(\vec{r}) e^{-W_n(t-t_0)} A_n + \dots, \end{aligned} \quad (10)$$

with constant $A_n = \langle W_n | \overline{\mathcal{J}^{(JP)}}(0) | 0 \rangle$, where $|W_n\rangle$ stands for an elastic scattering state with the energy of W_n , and the ellipses represent contributions from inelastic states.

2.1. Source operator

In this work, we choose a wall source at $t = t_0$ defined by

$$\mathcal{J}^{(JP)\text{wall}}(t_0) = P_{\beta\alpha}^{(JP)} \left[B_\alpha^{(1)\text{wall}}(t_0) B_\beta^{(2)\text{wall}}(t_0) \right], \quad (11)$$

where $P_{\beta\alpha}^{(JP)}$ is the projection operator to the total angular momentum J and the parity P . Here $B^{\text{wall}}(t_0)$ is obtained by replacing the local quark operator $q(\vec{x}, t)$ in the $B(\vec{x}, t)$ with the wall quark operator given by

$$q^{\text{wall}}(t_0) \equiv \sum_{\vec{x}} q(\vec{x}, t_0), \quad (12)$$

with the Coulomb gauge fixing at $t = t_0$. Since the orbital angular momentum of the wall source is fixed to $L = 0$, the source with fixed total angular momentum are obtained by the spin projection of the source. In the case of the $\Lambda_c N$ system, which has the total spin $S = 0$ or $S = 1$, the wall source operator $\mathcal{J}_{\Lambda_c N}^{(JP)\text{wall}}(t_0)$ with the spin projection to $S = 0$ or $S = 1$ creates the $\Lambda_c N$ system with $J^P = 0^+$ or $J^P = 1^+$, respectively.

2.2. Time dependent HAL QCD method

In principle, the baryon four-point correlation function is dominated by the NBS wave function of the ground state in the large time separation (Eq. (10)). In practice, however, it is difficult to realize the ground state domination since $t - t_0$ cannot be taken large enough due to statistical noises of the baryon four-point correlation function [27, 28, 29, 30]. This difficulty was overcome by the time-dependent HAL QCD method [31] as follows. Let us consider the normalized baryon four-point correlation function from Eq. (9) as

$$\begin{aligned} R_{\alpha\beta}(\vec{r}, t - t_0) &\equiv \frac{G_{\alpha\beta}(\vec{r}, t - t_0)}{e^{-m_{B(1)}(t-t_0)} e^{-m_{B(2)}(t-t_0)}} \\ &= \sum_n \psi_{\alpha\beta}^{(W_n)}(\vec{r}) e^{-\Delta W_n(t-t_0)} A_n + \dots, \end{aligned} \quad (13)$$

where $\Delta W_n = W_n - (m_{B(1)} + m_{B(2)})$, which satisfies

$$E_n \equiv \frac{k_n^2}{2\mu} = \Delta W_n + \frac{1 + 3\delta^2}{8\mu} (\Delta W_n)^2 + \mathcal{O}((\Delta W_n)^3), \quad (14)$$

where $\delta = (m_{B(1)} - m_{B(2)}) / (m_{B(1)} + m_{B(2)})$. Using the above relation and the Schrödinger equation in Eq. (6), we obtain

$$\left[\left(\frac{1 + 3\delta^2}{8\mu} \right) \frac{\partial^2}{\partial t^2} - \frac{\partial}{\partial t} - H_0 \right] R_{\alpha\beta}(\vec{r}, t - t_0) = \int d^3 r' U_{\alpha\beta; \alpha'\beta'}(\vec{r}, \vec{r}') R_{\alpha'\beta'}(\vec{r}', t - t_0), \quad (15)$$

for a moderately large $t - t_0$, where contributions from the inelastic states can be neglected. Although the higher order terms in Eq. (14) can be calculated by corresponding time derivative, those contributions turn out to be numerically negligible in the present lattice setup. The effects of higher derivative terms and the contribution from inelastic states are regarded as the systematic errors and estimated by the time dependence of scattering observables. It is noted that Eq. (15) becomes exact for $m_{B^{(1)}} = m_{B^{(2)}}$.

3. Lattice setup

For numerical simulations, we employ the (2+1)-flavor full QCD configurations generated by PACS-CS Collaboration [32] with the renormalization-group improved Iwasaki gluon action and a nonperturbatively $\mathcal{O}(a)$ improved Wilson-clover quark action at $\beta = 6/g^2 = 1.90$ on a $L^3 \times T = 32^3 \times 64$ lattice. The corresponding lattice spacing is $a = 0.0907(13)$ fm and physical lattice size is $La = 2.902(42)$ fm.

In order to see the quark mass dependence of the potentials, we employ three ensembles of gauge configurations. The hopping parameters of these ensembles are $\kappa_{ud} = 0.13700$ (Ensemble 1), 0.13727 (Ensemble 2), 0.13754 (Ensemble 3) for u, d -quarks while $\kappa_s = 0.13640$ (Each ensemble) for the s -quark. For the charm quark, we employ the relativistic heavy quark (RHQ) action [33] to avoid the leading $\mathcal{O}((m_Q a)^n)$ and the next-to-leading $\mathcal{O}((m_Q a)^n (a \Lambda_{\text{QCD}}))$ discretization errors due to the charm quark mass m_Q . We use the RHQ parameters determined in Ref. [34] so as to reproduce the experimental value of the mass and the relativistic dispersion relation for the charmonium in spin-averaged $1S$ state. Note that charm-quark loops are not considered in the present paper. The effects of charm loops for charmed baryons are expected to be small as studied e.g. in Ref. [35, 36]. Nevertheless, the effects to the $\Lambda_c N$ interaction is an interesting open question to be investigated in the future.

We calculate quark propagators with the periodic boundary condition for the spatial directions, while the Dirichlet boundary condition is imposed on the temporal direction at the time-slice $t = 32 + t_0$. Correlation functions for $\Lambda_c N$ are calculated using the unified contraction algorithm [37]. In order to increase the statistics, we take an average

over forward and backward propagations in time. Furthermore, we take 64 different time-slices for each configuration as the wall source location. The total statistics of each ensemble are given in Table 1.

Table 1: The number of configurations, sources, and masses of pion and nucleon on each ensemble. The factor of two in # of sources means forward and backward propagations in time.

	# of gauge configs.	# of sources	m_π [MeV]	m_N [MeV]
Ensemble 1	399	64×2	702(2)	1581(6)
Ensemble 2	400	64×2	570(1)	1399(9)
Ensemble 3	450	64×2	412(2)	1215(9)

For all analyses in this study, we employ the jackknife method to estimate statistical errors. The bin-size of the jackknife samples is taken to 57, 40 and 45 for the Ensemble 1, 2 and 3, respectively. We confirm that change of bin-size does not affect the errors for hadron masses as well as the errors for potentials and phase shifts.

Various hadron masses calculated in this work are summarized in Table 2.

4. Numerical results

4.1. $\Lambda_c N$ central potentials in 1S_0 channel

We first discuss the central potential for the S -wave spin-singlet $\Lambda_c N$ system. In order to obtain the potential, we use the R -correlator with the $J^P = 0^+$ wall source defined in Eq. (13), which is further projected to the 1S_0 channel as

$$R_{1S_0}(\vec{r}, t - t_0) \equiv P^{(L=0)} P_{\beta\alpha}^{(S=0)} R_{\alpha\beta}(\vec{r}, t - t_0; J^P = 0^+), \quad (16)$$

where $P_{\beta\alpha}^{(S=0)}$ and $P^{(L=0)}$ are projection operators to the total spin $S = 0$ and the orbital angular momentum $L = 0$, respectively¹. On the lattice, we employ the cubic

¹These projections are redundant since the $J^P = 0^+$ state allows only the 1S_0 channel.

Table 2: Calculated hadron masses in unit of [MeV] for each ensemble. The fit range in $t - t_0$ is [10, 20] for π in Ensemble 2, [10, 15] for π in Ensemble 3 and [15, 20] for all other cases.

	Ensemble 1	Ensemble 2	Ensemble 3
m_π	702(2)	570(1)	412(2)
m_K	789(2)	713(1)	637(2)
m_D	1999(1)	1949(2)	1904(2)
m_N	1581(6)	1399(9)	1215(9)
m_Λ	1642(6)	1493(7)	1342(6)
m_Σ	1657(6)	1522(8)	1395(9)
m_{Σ^*}	1881(11)	1749(16)	1631(28)
m_{Λ_c}	2685(3)	2555(5)	2434(6)
m_{Σ_c}	2780(5)	2674(7)	2575(9)
$m_{\Sigma_c^*}$	2866(5)	2763(7)	2661(10)

transformation group for the projection of the orbital angular momentum as

$$P^{(L=0)} R(\vec{r}, t - t_0) \equiv \frac{1}{24} \sum_{g \in SO(3, \mathbb{Z})} R(g^{-1} \vec{r}, t - t_0), \quad (17)$$

where g is one of 24 elements in $SO(3, \mathbb{Z})$. This projection picks up an A_1^+ representation of $SO(3, \mathbb{Z})$. By using the R -correlator in the 1S_0 channel, we extract the $\Lambda_c N$ central potential through Eq. (15). Since $\vec{\sigma}_1 \cdot \vec{\sigma}_2 = -3$ and $S_{12} = 0$ for the $J^P = 0^+$ state, we have

$$\begin{aligned} V_C^{(0+)}(\vec{r}) &\equiv V_0(\vec{r}) - 3V_\sigma(\vec{r}) \\ &= \frac{1}{R_{1S_0}(\vec{r}, t - t_0)} \left[\left(\frac{1 + 3\delta^2}{8\mu} \right) \frac{\partial^2}{\partial t^2} - \frac{\partial}{\partial t} - H_0 \right] R_{1S_0}(\vec{r}, t - t_0) \end{aligned} \quad (18)$$

for the moderately large $t - t_0$.

Fig. 1 shows the $\Lambda_c N$ central potential in the 1S_0 channel for each ensemble. The potential is calculated at $t - t_0 = 13$ (Ensemble 1: $m_\pi \simeq 700$ MeV), $t - t_0 = 11$ (Ensemble 2: $m_\pi \simeq 570$ MeV) and $t - t_0 = 9$ (Ensemble 3: $m_\pi \simeq 410$ MeV). We find a

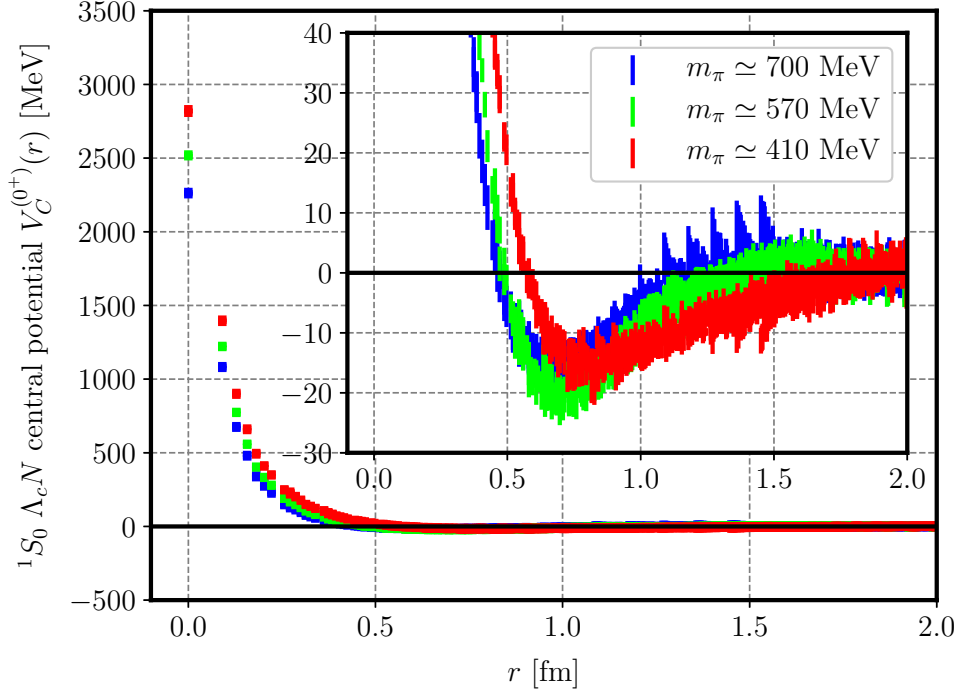


Figure 1: The $\Lambda_c N$ central potential in the 1S_0 channel for each ensemble. The potential is calculated at $t - t_0 = 13$ for $m_\pi \simeq 700$ MeV case (Blue), $t - t_0 = 11$ for $m_\pi \simeq 570$ MeV case (Green) and $t - t_0 = 9$ for $m_\pi \simeq 410$ MeV case (Red).

repulsive core at short distances ($r \lesssim 0.5$ fm) and an attractive pocket at intermediate distances ($0.5 \lesssim r \lesssim 1.5$ fm) in the $\Lambda_c N$ potential. We also observe that the height of the repulsive core increases and the minimum of the attractive pocket shifts outward, as u , d quark masses decrease. A variation of the repulsive core against u , d quark masses may be explained by the fact that the color magnetic interaction is proportional to the inverse of the constituent quark mass [38]. We notice that the attraction of the $\Lambda_c N$ potential seems weaker than that of the ΛN potential in Ref. [39].

In order to check the stability of the potential against the time separations $t - t_0$, we plot the time dependence of the $\Lambda_c N$ central potential in the 1S_0 channel at several different time separation $t - t_0$ in Fig. 2. In Fig. 2 (a), we find that the potential exhibits non-negligible time dependence for $t - t_0 \in [9, 12]$. The potential, however, becomes stable at larger time, $t - t_0 \in [13, 15]$, as shown in Fig. 2 (b). This observation

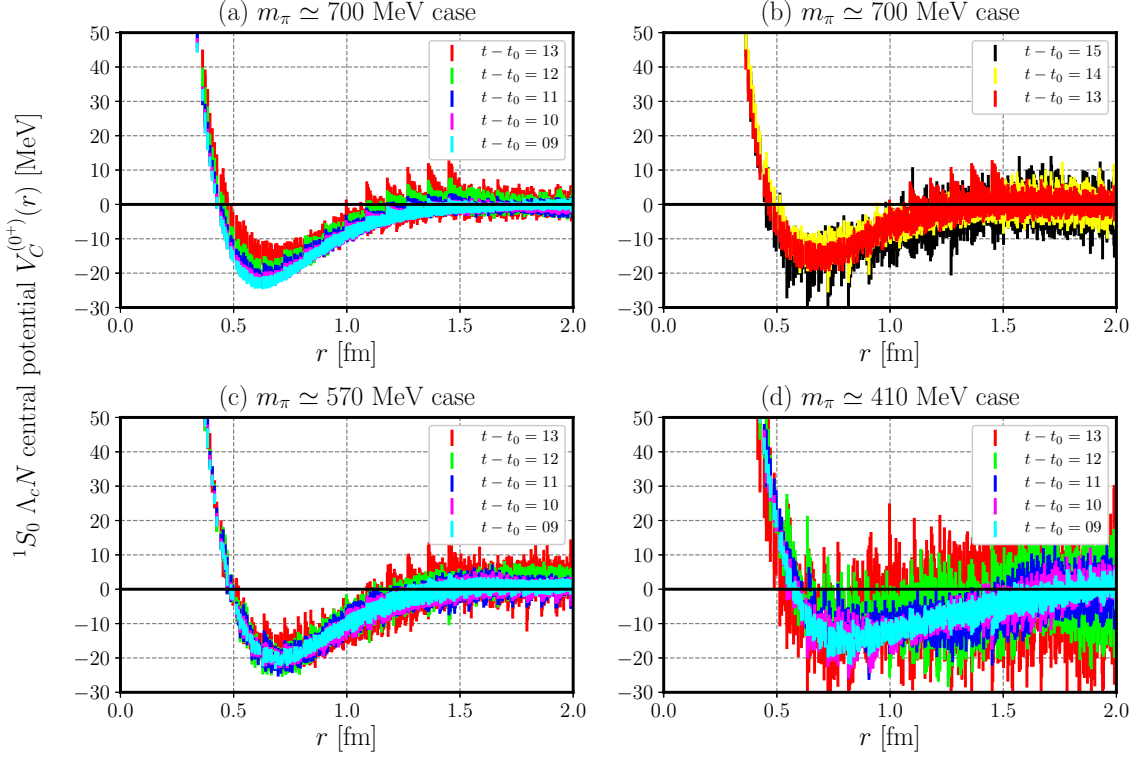


Figure 2: Time dependence of the $\Lambda_c N$ central potential in the 1S_0 channel for $m_\pi \simeq 700$ MeV case (a, b), $m_\pi \simeq 570$ MeV case (c) and $m_\pi \simeq 410$ MeV case (d).

suggests that contributions from inelastic states are negligible at $t - t_0 \geq 13$, so that we take the potential at $t - t_0 = 13$ for $m_\pi \simeq 700$ MeV case. For $m_\pi \simeq 570$ and 410 MeV cases, we find that potentials are stable within the statistical errors at earlier time slices ($t - t_0 \in [9, 13]$) as shown in Fig. 2 (c,d). This implies that the contaminations from inelastic states are more suppressed as ud quark masses are decreased: In fact, the excitation energy to the lowest inelastic state ($\Sigma_c N$) becomes larger for lighter ud quark masses. Another possible reason is that the statistical errors at fixed $t - t_0$ become larger for lighter quark masses and tend to dominate the total error budget compared to the systematic errors from inelastic states. Under these considerations, we take $t - t_0 = 11$ at $m_\pi \simeq 570$ MeV and $t - t_0 = 9$ at $m_\pi \simeq 410$ MeV in the following analyses.

We then calculate physical observables such as scattering phase shifts in the 1S_0

channel from the potential. For this purpose, we fit the potential data with the functional form given by

$$V_{\text{fit}}(r) = a_1 e^{-\left(\frac{r}{a_2}\right)^2} + a_3 e^{-\left(\frac{r}{a_4}\right)^2} + a_5 \left[\left(1 - e^{-a_6 r^2}\right) \frac{e^{-a_7 r}}{r} \right]^2. \quad (19)$$

Table 3 shows fit-parameters for the $\Lambda_c N$ central potential in the 1S_0 channel on each ensemble. Using data at $r \in (0.0, 2.0]$ fm, we achieve $\chi^2/\text{dof} \simeq 1$. We solve the

Table 3: Fit parameters of $V_{\text{fit}}(r)$ defined in Eq. (19) for the $\Lambda_c N$ (effective) central potential, where a_1 and a_3 are expressed in unit of [MeV], a_2 and a_4 are expressed in unit of [fm], a_5 , a_6 and a_7 are expressed in unit of [MeV fm²], [fm⁻²] and [fm⁻¹], respectively.

	1S_0 channel			3S_1 channel		
m_π	702(2) MeV	570(1) MeV	412(2) MeV	702(2) MeV	570(1) MeV	412(2) MeV
a_1	1090(36)	1266(20)	1520(24)	458.1(53.8)	682.6(13.4)	853.8(17.2)
a_2	0.09761(233)	0.09912(112)	0.1121(11)	0.09296(835)	0.1061(138)	0.1183(16)
a_3	854.4(50.2)	892.5(27.3)	712.4(12.8)	761.6(71.8)	631.0(17.5)	569.2(11.2)
a_4	0.4384(45)	0.4670(36)	0.6808(51)	0.4208(59)	0.4886(32)	0.6898(56)
a_5	-18637(5796)	-29804(6231)	-45479(4116)	-71142(38550)	-19158(3687)	-40798(3994)
a_6	1.566(154)	1.182(84)	0.6635(229)	0.8462(1626)	1.163(77)	0.6144(221)
a_7	3.493(122)	3.308(74)	2.367(25)	3.971(164)	3.071(66)	2.331(27)

Schrödinger equation with the fitted potential in the infinite volume and extract its phase shifts from the asymptotic behavior of the wave function. Finally, the S -wave scattering length is calculated as

$$a = \lim_{k \rightarrow 0} \frac{\tan \delta_{00}(k)}{k}. \quad (20)$$

Here we employ the particle physics convention for the definition of scattering length which has opposite sign from the historical sign convention of the baryon-baryon interaction.

Fig. 3 show the phase shift and the scattering length for the $\Lambda_c N$ system in the 1S_0 channel for each ensemble, and the numerical values of the scattering length are listed

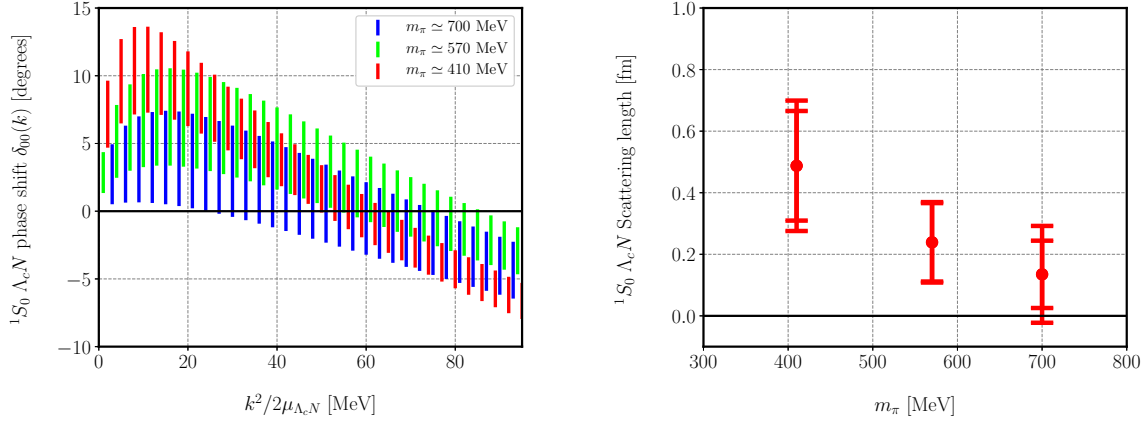


Figure 3: The phase shift (left) and the scattering length (right) for the $\Lambda_c N$ system in the 1S_0 channel with particle physics sign convention of the scattering length. The inner error of the scattering length is statistical only, while the outer represents the total one (statistical and systematic errors added in quadrature).

in Table 4. Systematic errors of the scattering length are evaluated by the difference between the mean value at $t - t_0$ and that at $t - t_0 + 2$, where $t - t_0 = 13, 11$ and 9 for $m_\pi \simeq 700, 570$ and 410 MeV case, respectively. Results of these observables indicate that the net interaction in the 1S_0 channel is attractive at low energies ($E \lesssim 40$ MeV) in all cases, but not strong enough to form bound states. We also notice a tendency that the attraction becomes stronger as the pion mass decreases ².

The leading order approximation of the $\Lambda_c N$ potential may have sizable systematic errors once E approaches to the $\Sigma_c N$ threshold from below ($E \simeq 96, 121$ and 145 MeV for $m_\pi \simeq 700, 570$ and 410 MeV case, respectively) due to the truncation of the derivative expansion of the non-local potential. Such systematic uncertainties of the

²We have reported preliminary results of the $\Lambda_c N$ potential at $t - t_0 = 9$ in Ref. [40] and those at $t - t_0 = 10$ in Ref. [41]. Since we have more statistics than those preliminary studies, we could analyze the potential at larger $t - t_0$ in the present paper. As a consequence, together with the large statistical fluctuation observed at $m_\pi \simeq 410$ MeV in the 3S_1 channel, the preliminary results show an opposite tendency in terms of the quark mass dependence of the scattering lengths.

Table 4: The scattering length for the $\Lambda_c N$ system with the particle physics sign convention. The first parenthesis indicates the statistical error, and the second parentheses indicates the systematic error evaluated by the difference between the mean value at $t - t_0$ and that at $t - t_0 + 2$.

m_π	1S_0 channel	3S_1 channel
412(2) MeV	0.49 (18) (11) fm	0.51 (20) (9) fm
570(1) MeV	0.24 (13) (3) fm	0.29 (16) (9) fm
702(2) MeV	0.13 (11) (11) fm	0.17 (10) (12) fm

$\Lambda_c N$ interaction near the $\Sigma_c N$ threshold can be estimated by comparing the phase shift calculated by the leading order potential and that obtained by the coupled-channel potential [19, 23]. Our preliminary results of the coupled-channel potential in Ref. [41] indicate that the phase shifts obtained by the two methods in the 3S_1 channel for $\Lambda_c N$ system agree with each other even near the $\Sigma_c N$ threshold. More systematic study with both 3S_1 and 1S_0 channels are needed to draw quantitative conclusion.

4.2. $\Lambda_c N$ central and tensor potentials in $^3S_1 - ^3D_1$ channel

The $J^P = 1^+$ wall source in Eq. (11) generates states in the 3S_1 channel at t_0 , but the R -correlator contains both 3S_1 and 3D_1 channels at $t > t_0$ due to QCD interactions. This fact is translated into the existence of the tensor potential, which is the transition potential between these two channels. To extract both central and tensor potentials, we introduce the projections to the S -wave and D -wave components as

$$\begin{aligned}
P_S R_{\alpha\beta}(\vec{r}, t - t_0) &\equiv P^{(L=0)} R_{\alpha\beta}(\vec{r}, t - t_0) \\
P_D R_{\alpha\beta}(\vec{r}, t - t_0) &\equiv (1 - P^{(L=0)}) R_{\alpha\beta}(\vec{r}, t - t_0),
\end{aligned} \tag{21}$$

where $P^{(L=0)}$ is the projection operator defined in Eq. (17). Using Eq. (21), both central and tensor potentials are extracted from the coupled channel Schrödinger equation as

$$\begin{aligned}\mathcal{K} [P_S R_{\alpha\beta}(\vec{r}, t - t_0)] &= V_C^{(1+)}(\vec{r}) [P_S R_{\alpha\beta}(\vec{r}, t - t_0)] + V_T(\vec{r}) \left[P_S (S_{12} R)_{\alpha\beta}(\vec{r}, t - t_0) \right], \\ \mathcal{K} [P_D R_{\alpha\beta}(\vec{r}, t - t_0)] &= V_C^{(1+)}(\vec{r}) [P_D R_{\alpha\beta}(\vec{r}, t - t_0)] + V_T(\vec{r}) \left[P_D (S_{12} R)_{\alpha\beta}(\vec{r}, t - t_0) \right],\end{aligned}\quad (22)$$

where \mathcal{K} is the operator in the left-hands of Eq. (15), given by

$$\mathcal{K} \equiv \left(\frac{1 + 3\delta^2}{8\mu} \right) \frac{\partial^2}{\partial t^2} - \frac{\partial}{\partial t} - H_0, \quad (23)$$

and the central potential with $J^P = 1^+$ is expressed as

$$V_C^{(1+)}(\vec{r}) = V_0(\vec{r}) + V_\sigma(\vec{r}), \quad (24)$$

since $(\vec{\sigma}_1 \cdot \vec{\sigma}_2) = +1$.

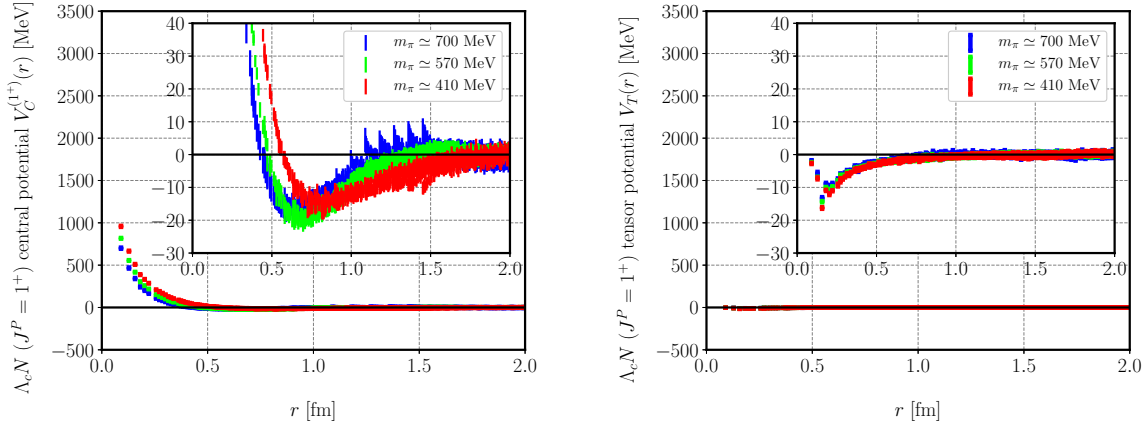


Figure 4: $\Lambda_c N$ central potential (left) and tensor potential (right) in the $J^P = 1^+$ state for each ensemble. The potentials are calculated at $t - t_0 = 13$ for $m_\pi \simeq 700$ MeV case (Blue), $t - t_0 = 11$ for $m_\pi \simeq 570$ MeV case (Green) and $t - t_0 = 9$ for $m_\pi \simeq 410$ MeV case (Red).

Fig. 4 shows that the central potential (left) and the tensor potential (right) for the $\Lambda_c N$ system with $J^P = 1^+$. These potentials are calculated at $t - t_0 = 13$ (Ensemble 1: $m_\pi \simeq 700$ MeV), $t - t_0 = 11$ (Ensemble 2: $m_\pi \simeq 570$ MeV) and $t - t_0 = 9$ (Ensemble

3: $m_\pi \simeq 410$ MeV). It is confirmed that these potentials are stable against the change of $t - t_0$ within the statistical errors, as was observed in the central potential in the 1S_0 channel. We notice that the central potential is similar to the one in the 1S_0 channel except at short distances ($r \lesssim 0.5$ fm). The tensor potential of the $\Lambda_c N$ system is weak compared to that of the ΛN system [39]. We also find that the u , d quark mass dependence of the tensor potentials is weak.

The weaker $\Lambda_c N$ potential than ΛN could be explained from following facts: (i) The long-range contribution is expected to be caused by the K meson exchange for ΛN interaction [6]. In the $\Lambda_c N$ system, however, the K meson (strange quark) exchange is replaced by the D meson (charm quark) exchange, and this contribution is highly suppressed due to the much heavier D meson mass than the K meson mass. (ii) The one-pion exchange in the $\Lambda N - \Sigma N$ transition is considered to give a sizable contribution to the effective ΛN interaction. In the $\Lambda_c N$ system, however, this contribution is expected to be suppressed due to the large mass difference between $\Lambda_c N$ and $\Sigma_c N$.

By the same procedure as in the case of the 1S_0 , we calculate the phase shifts and the scattering lengths in this system. Since the tensor potential is shown to be weak, we employ the effective central potential in the 3S_1 channel (instead of the $^3S_1 - ^3D_1$ coupled channel), which implicitly includes the effect of the tensor potential through virtual processes such as $^3S_1 \rightarrow ^3D_1 \rightarrow ^3S_1$. The $\Lambda_c N$ effective-central potential is plotted in Fig. 5, and fit parameters are given in Table 3. The phase shift and the scattering length shown in Fig. 6 are very similar to those in the 1S_0 channel. See also Table 4 for a comparison of the scattering length between two channels.

4.3. Spin independence of central potentials

In this subsection, we quantify a similarity between the 1S_0 central potential and the 3S_1 effective central potential. For this purpose, we further decompose the central potential in both $J^P = 0^+$ state (Eq. 18) and $J^P = 1^+$ state (Eq. 24) into the spin-independent central potential V_0 and the spin-dependent one V_σ , which are extracted

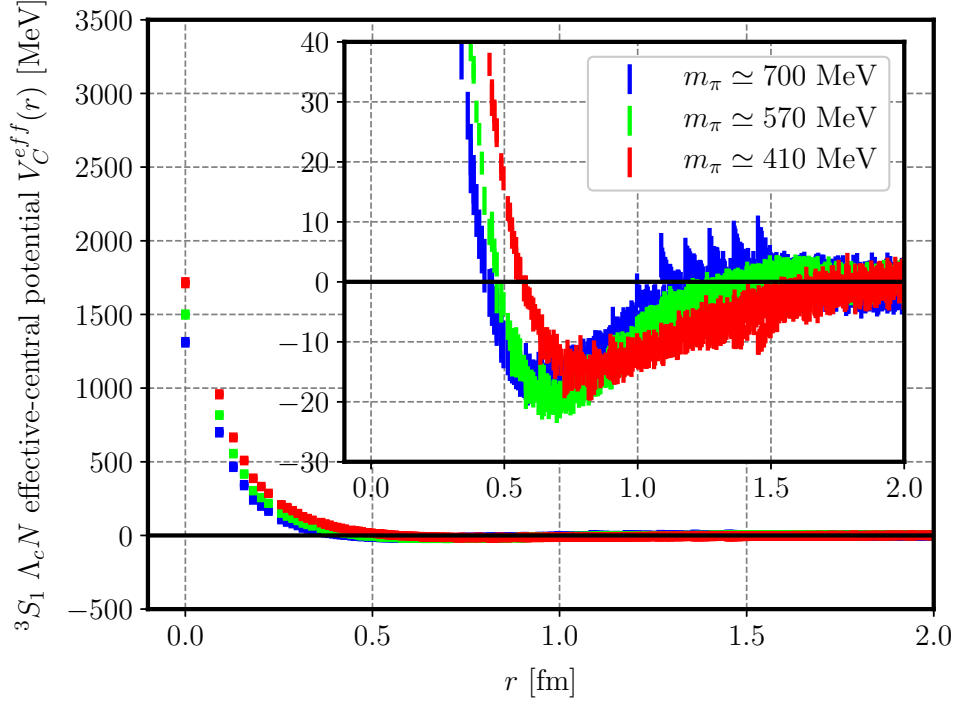


Figure 5: The $\Lambda_c N$ effective-central potential in the 3S_1 channel for each ensemble. The potential is calculated at $t - t_0 = 13$ for $m_\pi \simeq 700$ MeV case (Blue), $t - t_0 = 11$ for $m_\pi \simeq 570$ MeV case (Green) and $t - t_0 = 9$ for $m_\pi \simeq 410$ MeV case (Red).

as

$$V_0(\vec{r}) = \frac{1}{4} \left(3V_C^{(1+)}(\vec{r}) + V_C^{(0+)}(\vec{r}) \right) \quad (25)$$

$$V_\sigma(\vec{r}) = \frac{1}{4} \left(V_C^{(1+)}(\vec{r}) - V_C^{(0+)}(\vec{r}) \right). \quad (26)$$

Fig. 7 shows the $\Lambda_c N$ spin-independent central potential V_0 (left) and the spin-dependent one V_σ (right). It is easy to see that the spin-dependent potential V_σ is negligibly small, and the spin-independent central potential gives a significant contribution for $\Lambda_c N$ potentials. The origin of the small spin-dependent potential V_σ could be explained by the heavy D-meson mass and the large separation between $\Lambda_c N$ and $\Sigma_c N$, similar to the case of $\Lambda_c N$ tensor potential in 3S_1 - 3D_1 channel.

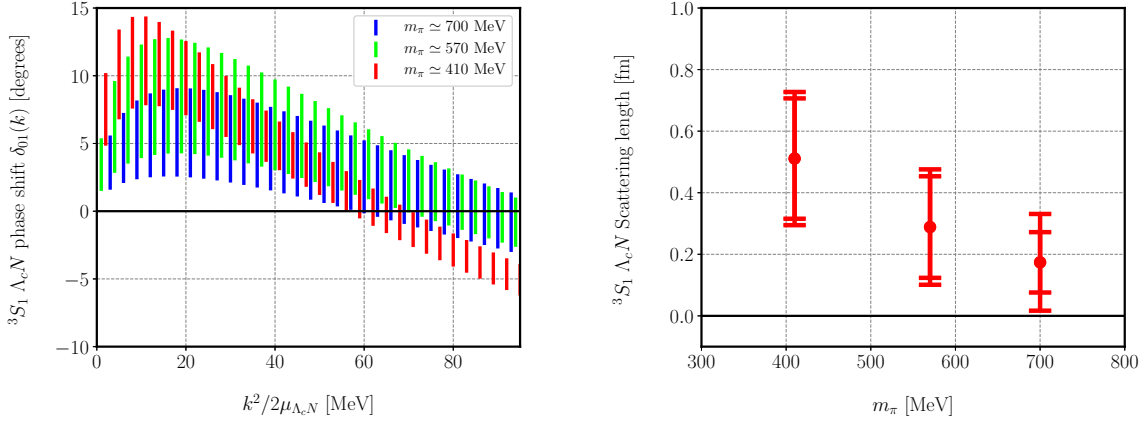


Figure 6: The phase shifts (left) and the scattering length (right) for the $\Lambda_c N$ system in the 3S_1 channel with particle physics sign convention of the scattering length. The inner error of the scattering length is statistical only, while the outer represents the total one (statistical and systematic errors added in quadrature).

5. Possible Λ_c hypernuclei

Since the $\Lambda_c N$ interaction is dominated by the spin-independent central force, as we discussed in the previous section, the spectrum of Λ_c hypernuclei, if they exist, would be simple. In order to investigate Λ_c hypernuclei, we employ the single-folding potential defined by

$$V_F(\vec{r}) = \int d^3r' \rho_A(\vec{r}') V_{\Lambda_c N}(\vec{r} - \vec{r}'), \quad (27)$$

where $\rho_A(\vec{r})$ denotes nuclear density distributions with the atomic number A , and $V_{\Lambda_c N}(\vec{r}) = V_0(\vec{r})$ stands for the two body spin-independent central potential of the $\Lambda_c N$ system.

For the nuclear density distribution function, we use the two-parameter Fermi form given by

$$\rho_A(\vec{r}) = \rho_0 \left[1 + \exp\left(\frac{r - c}{a}\right) \right]^{-1}, \quad \int d^3r \rho_A(\vec{r}) = A, \quad (28)$$

where $r \equiv |\vec{r}|$. We employ the parameters ρ_0 , c , a given in Ref. [42] for spherical nuclei such as ^{12}C , ^{28}Si , ^{40}Ca , ^{58}Ni , ^{90}Zr and ^{208}Pb .

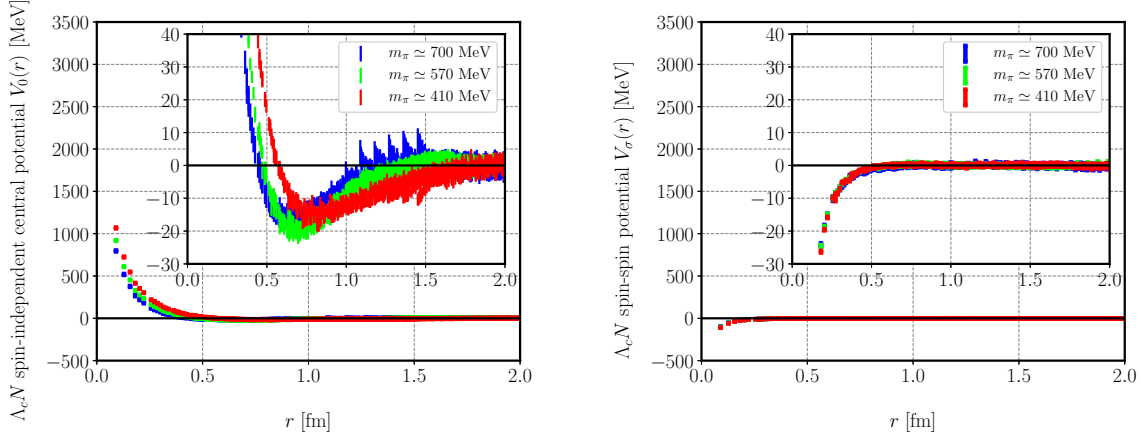


Figure 7: $\Lambda_c N$ spin-independent central potential V_0 (left) and the spin-dependent one V_σ (right) for each ensemble. The potentials are calculated at $t - t_0 = 13$ for $m_\pi \simeq 700$ MeV case (Blue), $t - t_0 = 11$ for $m_\pi \simeq 570$ MeV case (Green) and $t - t_0 = 9$ for $m_\pi \simeq 410$ MeV case (Red).

Fig. 8 shows the folding potential for $\Lambda_c - {}^{208}\text{Pb}$ for each ensemble. We observe that the folding potential becomes deeper as the u , d quark masses decrease and becomes as large as -10 to -20 MeV at the origin.

Using this folding potential, we calculate the binding energy of the Λ_c hypernuclei by the Gaussian expansion method [43] for the S -wave potential, with the physical masses for Λ_c and nuclei. Fig. 9 shows the binding energy of several Λ_c hypernuclei for each ensemble. As we expected, the binding energy $|E_b|$ increases as the atomic number increases. Furthermore, as the $\Lambda_c N$ potential approaches to the physical one (as the u , d quark masses decrease toward physical values), the binding energy increases. These results suggest that Λ_c hypernuclei may exist, if their binding energy is larger than the Coulomb repulsion. In order to estimate the effect of Coulomb force, we calculate the expectation value for the Coulomb potential using the binding solutions of Λ_c hypernuclei $|\psi_b\rangle$ as

$$E_{\text{Coulomb}} = \frac{\langle \psi_b | V_F^C | \psi_b \rangle}{\langle \psi_b | \psi_b \rangle}, \quad (29)$$

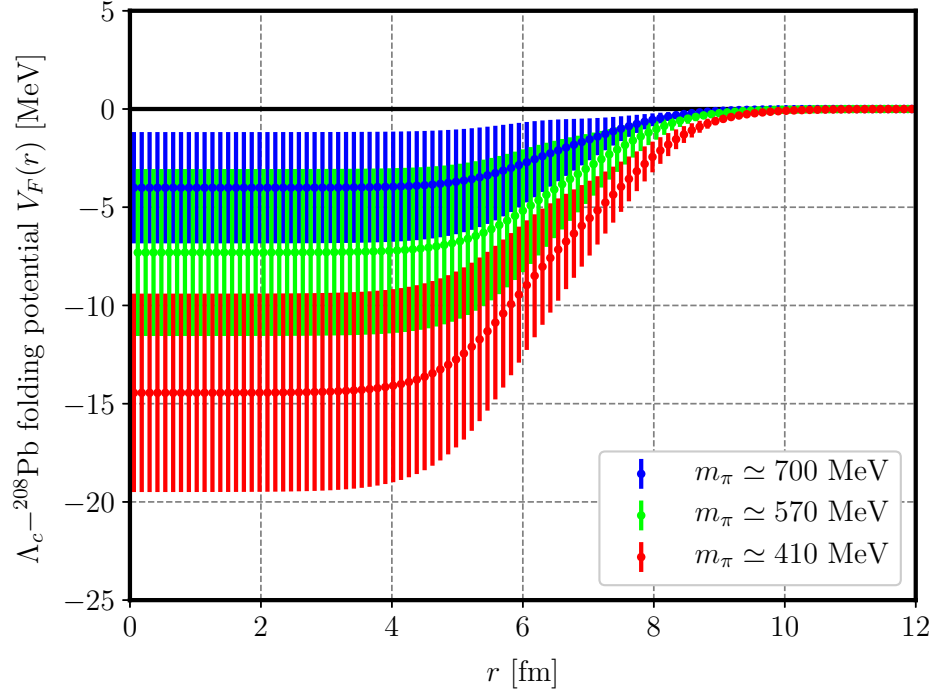


Figure 8: Λ_c - ^{208}Pb folding potentials calculated from the spin-independent central potential of the $\Lambda_c N$ system (Fig. 7) for $m_\pi \simeq 700, 570$ and 410 MeV cases.

where V_F^C is the single-folding Coulomb potential defined by

$$V_F^C(\vec{r}) = \int d^3r' \rho_{\text{ch}}(\vec{r}') V_{\text{Coulomb}}(\vec{r} - \vec{r}'), \quad (30)$$

where $V_{\text{Coulomb}}(\vec{r})$ is an ordinary Coulomb potential and ρ_{ch} is charge density distribution by the Fourier-Bessel coefficient obtained from elastic electron scattering [44]. Fig. 10 shows the expectation values of the folding potential for Coulomb force calculated by using the binding solution of Λ_c hypernuclei for Ensemble 3 ($m_\pi \simeq 410$ MeV). For comparison, we also plot the binding energy for Λ_c hypernuclei without Coulomb potential and the sum of them in Fig. 10. We observe that the Coulomb repulsion is large for heavy nuclei and Λ_c - ^{208}Pb state becomes unbound with Coulomb force. In the nuclei for $A = 12 - 58$, on the other hand, the expectation values of Coulomb force are not much stronger than the binding energy of Λ_c hypernuclei. Since the binding energy increases as the attraction of the $\Lambda_c N$ potential becomes stronger toward the

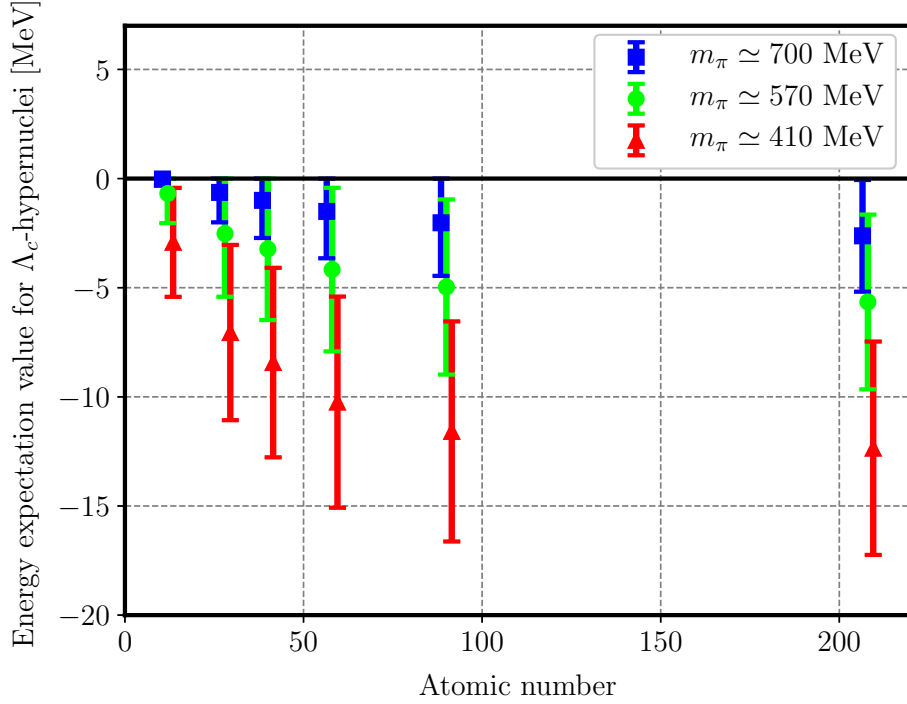


Figure 9: The binding energy of Λ_c in symmetric nuclei such as ^{12}C , ^{28}Si , ^{40}Ca , ^{58}Ni , ^{90}Zr and ^{208}Pb for each ensemble. The binding energies are calculated from the folding potentials for Λ_c hypernuclei by using the Gaussian expansion method. The folding potentials are constructed from the spin-independent central potential of the $\Lambda_c N$ system (Fig. 7) for $m_\pi \simeq 700$, 570 and 410 MeV cases. In the calculation of the binding energies, we adjust the mass of Λ_c and nuclei to those of physical values.

physical quark mass, this observation suggests a possibility that Λ_c hypernuclei may exist in light or medium-heavy nuclei.

6. Summary and conclusions

We have investigated the $\Lambda_c N$ interaction on the basis of lattice QCD simulations. The potentials have been extracted by the HAL QCD method using the (2+1)-flavor full QCD configurations with the lattice volume of $(2.9 \text{ fm})^3$ and the pion mass, $m_\pi \simeq 410, 570, 700$ MeV. We have extracted the central potential in 1S_0 channel and the central and tensor potential in 3S_1 – 3D_1 channel. We found a repulsion at short distances and an attraction at intermediate distances in the central potentials for both

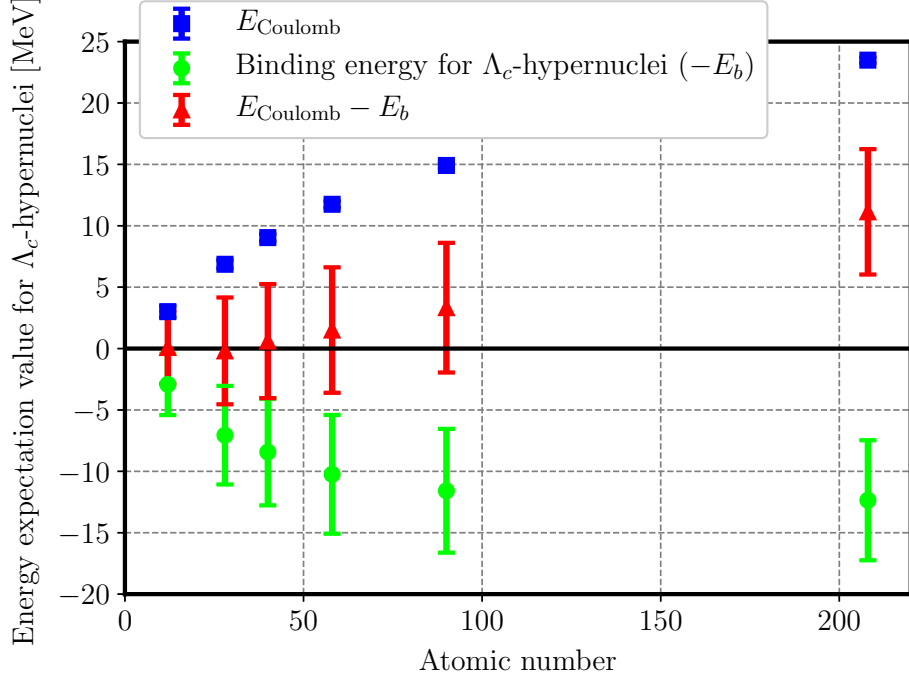


Figure 10: The expectation value of folding potential for Coulomb force in Λ_c hypernuclei (Blue). The expectation values are calculated from the binding solution of the Λ_c hypernuclei for Ensemble 3 ($m_\pi \simeq 410$ MeV). For comparison, the binding energy of Λ_c hypernuclei (Green) and sum of them (Red) are also plotted.

channels. The strength of the attraction is weaker than that in the ΛN potential, which is consistent with phenomenological model calculations [3, 6]. For the tensor potential, we found that the strength is weaker compared with that for the ΛN system.

We next calculated phase shifts and scattering lengths using the potential fitted to the lattice data. The results show that the $\Lambda_c N$ interaction is attractive at low energies ($E \lesssim 40$ MeV) in both 1S_0 and $^3S_1 - ^3D_1$ channels with comparable strength. In order to quantify the similarity of potentials between two channels, we decomposed the central potentials into the spin-independent and spin-dependent ones. We found that the spin-dependent potential is negligibly weak except at short distances.

The dominant contribution of the $\Lambda_c N$ interaction comes from the spin-independent central potential, from which we have constructed a single-folding potential for Λ_c

hypernuclei. We then estimated the binding energies of Λ_c with the nuclei, ^{12}C , ^{28}Ni , ^{40}Ca , ^{58}Ni , ^{90}Zr and ^{208}Pb , by using the Gaussian expansion method. Resultant binding energies of Λ_c hypernuclei become larger as the atomic number increases and/or the u , d quark mass decreases. In order to estimate the effect of the Coulomb repulsion in the Λ_c hypernuclei, we calculated expectation values of the folding potential of Coulomb force using the binding solution of Λ_c hypernuclei. The expectation value of the Coulomb potential is larger than the binding energy of Λ_c hypernuclei for heavy nuclei, while that is comparable to the binding energies from QCD for the nuclei with $A = 12 - 58$. These suggest possible Λ_c hypernuclei with light or medium-heavy nuclei in the real world.

Currently, we plan to carry out full QCD simulations near the physical quark masses by using gauge configurations generated by K-computer in AICS, RIKEN. This may make it possible to draw definite conclusions on the $\Lambda_c N$ interactions and Λ_c hypernuclei. We also plan to investigate the inelastic contributions for $\Lambda_c N$ interactions on the basis of the coupled-channel HAL QCD method [19, 23]. It is also an interesting future problem to study interactions in other two-body systems such as $\Lambda_c \Lambda_c$ and $\Xi_c N$, in order to understand the nature of charmed baryon interactions.

Acknowledgments

The author thanks all the members of the HAL QCD Collaboration for discussion. The author is also grateful to Shigehiro Yasui and Yasuhiro Yamaguchi for fruitful discussions and comments. This work is supported in part by the Grant-in-Aid of the Japanese Ministry of Education, Sciences and Technology, Sports and Culture (MEXT) for Scientific Research (No. JP15K17667, JP16H03978, JP17K14287, (C)26400281), by a priority issue (Elucidation of the fundamental laws and evolution of the universe) to be tackled by using Post “K” Computer, and by Joint Institute for Computational Fundamental Science (JICFuS). T.D. and T.H. are partially supported by RIKEN iTHES Project and iTHEMS Program. S.G is supported by the Special Postdoctoral Researchers Program of RIKEN. We thank the PACS-CS Collaboration for providing

us their $2 + 1$ flavor gauge configurations [32]. Numerical computations of this work have been carried out by the KEK supercomputer system (BG/Q), [Project number : 14/15-21, 15/16-12].

References

- [1] R. Machleidt and I. Slaus, J. Phys. G **27** (2001) R69
- [2] E. Hiyama, T. Motoba, T. A. Rijken and Y. Yamamoto, Prog. Theor. Phys. Suppl. **185** (2010) 1.
- [3] C. B. Dover and S. H. Kahana, Phys. Rev. Lett. **39** (1977) 1506.
- [4] C. B. Dover *et al.* Phys. Rev. **D16** (1977) 799-815.
- [5] H. Bando and M. Bando, Phys. Lett. **B109**, 164 (1982).
- [6] H. Bando and S. Nagata, Prog. Theor. Phys. **69**, 557 (1983).
- [7] H. Bando, Prog. Theor. Phys. Suppl. **81**, 197 (1985).
- [8] Y. R. Liu, M. Oka, Phys. Rev. **D85** (2012) 014015, [arXiv:1103.4624 [hep-ph]].
- [9] H. Huang, J. Ping, and F. Wang, Phys. Rev. **C87**, 034002 (2013).
- [10] Gal, A. *et al.* Phys. Rev. **D90** (2014) no.1, 014019, [arXiv:1405.5094 [nucl-th]].
- [11] S. Maeda, M. Oka, A. Yokota, E. Hiyama and Y. R. Liu, PTEP **2016** (2016) no.2, 023D02.
- [12] H. Garcilazo, A. Valcarce and T. F. Caramés, Phys. Rev. **C92** (2015) no.2, 024006.
- [13] K. Tsushima and F. C. Khanna, Phys. Rev. **C67** (2003) 015211.
- [14] K. Tsushima and F. C. Khanna, J. Phys. G: Nucl. Part. Phys. **30** (2004) 1765-1786.
- [15] N. Ishii, S. Aoki and T. Hatsuda, Phys. Rev. Lett. **99** (2007) 022001 [nucl-th/0611096].

- [16] S. Aoki, T. Hatsuda and N. Ishii, Prog. Theor. Phys. **23** (2010) 89 [arXiv:0909.5585 [hep-lat]].
- [17] S. Aoki *et al.* [HAL QCD Collaboration], Prog. Theor. Exp. Phys. **2012** (2012) 01A105 [arXiv:1206.5088 [hep-lat]].
- [18] T. Inoue *et al.* [HAL QCD Collaboration], Phys. Rev. Lett. **106** (2011) 162002 [arXiv:1012.5928 [hep-lat]].
- [19] S. Aoki *et al.* [HAL QCD Collaboration], Proc. Jpn. Acad., Ser. B, **87** (2011) 509 [arXiv:1106.2281 [hep-lat]].
- [20] T. Doi *et al.* [HAL QCD Collaboration], Prog. Theor. Phys. **127** (2012) 723.
- [21] K. Murano *et al.* [HAL QCD Collaboration], Phys. Lett. **B735** (2014) 19 [arXiv:1305.2293 [hep-lat]].
- [22] Y. Ikeda *et al.* [HAL QCD Collaboration], Phys. Lett. **B729** (2014) [arXiv:1311.6214 [hep-lat]].
- [23] K. Sasaki *et al.* Prog. Theor. Exp. Phys. (2015) 113B01 [arXiv:1504.01717 [hep-lat]].
- [24] T. Inoue *et al.* [HAL QCD Collaboration], PoS **CD15** (2016) 020 [arXiv:1511.04871 [hep-lat]].
- [25] Okubo S., Marshak R. E., Ann. Phys. 4, 166 (1958).
- [26] K. Murano *et al.* [HAL QCD Collaboration], Prog. Theor. Phys. **125**, 1225 (2011), [arXiv:1012.3814v1 [hep-lat]].
- [27] T. Iritani *et al.* [HAL QCD Collaboration], JHEP **1610**, 101 (2016) [arXiv:1607.06371 [hep-lat]].
- [28] S. Aoki [HAL QCD Collaboration], PoS LATTICE **2016**, 109 (2016) [arXiv:1610.09763 [hep-lat]].

- [29] T. Iritani [HAL QCD Collaboration], PoS LATTICE **2016**, 107 (2016) [arXiv:1610.09779 [hep-lat]].
- [30] T. Iritani *et al.* [HAL QCD Collaboration], Phys. Rev. **D96** (2017) no.3, 034521 [arXiv:1703.07210 [hep-lat]].
- [31] N. Ishii *et al.* [HAL QCD Collaboration], Phys. Lett. **B712** (2012) 437 [arXiv:1203.3642 [hep-lat]].
- [32] PACS-CS Collaboration: S. Aoki, *et al.*, Phys. Rev. **D79** (2009) 034503.
- [33] S. Aoki, Y. Kuramashi and S. Tominaga, Prog. Theor. Phys. **109** (2003) 383. [arXiv:hep-lat/0107009].
- [34] Y. Namekawa, *et al.* (PACS-CS Collaboration), Phys. Rev. **D87**, 094512 [arXiv:1301.4743 [hep-lat]].
- [35] Mattia Bruno, Jacob Finkenrath, Francesco Knechtli, Björn Leder, and Rainer Sommer (ALPHA collaboration), Phys. Rev. Lett. **114** (2015) 102001 [arXiv:1410.8374 [hep-lat]].
- [36] Francesco Knechtli, Andreas Athenodorou, Mattia Bruno, Jacob Finkenrath, Björn Leder, Marina Marinkovic, Rainer Sommer, PoS LATTICE **2014** (2014) 288 [arXiv:1411.1239 [hep-lat]].
- [37] T. Doi and M. G. Endres, Comput. Phys. Commun. **184**, 117 (2013) [arXiv:1205.0585 [hep-lat]].
- [38] M. Oka, K. Shimizu, and K. Yazaki, Nucl. Phys. **A464** (1987) 700.
- [39] H. Nemura *et al.* [HAL QCD Collaboration], PoS LATTICE **2011** (2011) 167 [arXiv:1203.3320 [hep-lat]].
- [40] T. Miyamoto *et al.* [HAL QCD Collaboration], PoS LATTICE **2015** (2016) 090 [arXiv:1602.07797 [hep-lat]].

- [41] T. Miyamoto *et al.* [HAL QCD Collaboration], PoS LATTICE **2016** (2017) 117.
- [42] M. El-Azab Farid and M.A. Hassanain, Nucl. Phys. **A678** (2000) 39.
- [43] E. Hiyama, Y. Kino and M. Kamimura, Prog. Part. Nucl. Phys. **51** (2003) 223.
- [44] H. De Vries, C. W. De Jager, and C. De Vries, Atomic Data and Nuclear Data Tables. **36** (1987) 495-536